# Simplified Polarization Estimation Using Co-Located Antennas

**Hui Li[1, 2, *], Miao Wu[1], Yibo Cheng[1], and Fei Wu[2]**

**Abstract**—Estimating polarization information using vector antennas is of great significance in signal processing. However, the antenna patterns are normally assumed ideal without considering practical factors, such as cross polarization. Moreover, pattern calibration is required in data processing. In this work, we first illustrate the polarization estimation method, taking into account the cross polarization of antennas. To simplify the estimation, we introduce a practical co-located antenna pair comprising a sleeve monopole and a windmill loop, which share mostly identical radiation patterns but orthogonal polarizations. The cross polarizations of both antennas are below $-20$ dB. Besides, the phase and amplitude patterns of both antennas are almost omnidirectional in the azimuth plane, avoiding complicated calibrations. Attributed to orthogonal polarizations, good isolation is achieved, and the envelope correlation coefficient is below 0.01. With the proposed antenna, the axial ratio and phase difference of the incoming wave are reasonably estimated without pattern calibration and compensation. The co-located antenna pair was fabricated, using which the polarization information of a commercial WLAN antenna has been measured.

## 1. INTRODUCTION

Direction finding and polarization estimation have received great attention in both military and civil applications, such as radar [1] and terminal localization [2]. To obtain the direction of arrival (DOA), spatially distributed antenna arrays are normally used, which occupy a large area [3, 4]. By contrast, employing vector antennas consisting of electric and magnetic dipoles can reduce the volume of the system, and meanwhile enable the capability of polarization estimation.

Estimating DOA and polarization using vector sensors originates from signal processing, where isotropic radiation patterns are normally assumed for the dipole and loop antennas. However, the actual patterns deviate a lot from being isotropic, and the deviation has great effect on the estimation accuracy. Thus, pattern compensations should be performed in signal processing. In [5], pattern compensation is carried out using the analytical formula of the patterns for infinitely small dipoles and loops [6], which is not practical for real antennas, either.

In the literature [7–11], the methods to obtain polarization information have been investigated and compared, using the combinations of dipoles or loops. Still electrically small antennas are assumed, which have small input impedance and form inefficient radiators. An input resistance of less than 0.001 ohms has been observed for the small loop in [12]. When the small loop is modified for better impedance matching, its radiation pattern deviates from the typical omnidirectional pattern, and the cross polarization increases [13]. To avoid using electrically small antennas, [14] and [15] develop algorithms to estimate the polarization information with electrically large dipoles and loops, respectively. Till now, polarization estimation is mainly studied in the field of signal processing, and few study has been carried out on building real antennas and measuring the polarization in practice. Loop antenna

\* Corresponding author: Hui Li (hui.li@dlut.edu.cn).
[1] School of Information and Communication Engineering, Dalian University of Technology, Dalian 116024, China. [2] Zhongshan Hospital of Dalian University, Dalian 116001, China.

and vertical dipole arrays in a centered conducting cylinder are designed for polarization estimation in [16], but the estimation accuracy is quite limited. In [17], a reconfigurable grounded vector antenna has been proposed. Omnidirectional patterns are obtained in the simulation with ideal infinite ground plane, whereas the undesirable ripples appear for finite ground plane in practice. [18] provides a pair of electric dipole and loop antennas for polarization diversity without considering the phase pattern. Furthermore, the 3D structure of the loop is difficult to fabricate, and the balun for the dipole distorts the radiation pattern slightly.

## 2. METHOD OF ESTIMATION

As denoted in Fig. 1, the electric field of an incoming signal is described by $E_\theta$ and $E_\varphi$ components as:

$$\mathbf{E} = E_\theta \mathbf{a_\theta} + E_\varphi \mathbf{a_\varphi} = E\left(\sin\gamma e^{j\eta}\mathbf{a_\theta} + \cos\gamma\mathbf{a_\varphi}\right), \tag{1}$$

where $\eta$ is the phase difference between $E_\theta$ and $E_\varphi$ component, and $\tan\gamma$ is the amplitude ratio. $\eta$ and $\gamma$ are in the range of $-\pi \leq \eta < \pi$ and $0 \leq \gamma \leq \pi/2$, respectively. Ideally, the small dipole and loop antennas receive only $E_\theta$ and $E_\varphi$ components, respectively, so that the signals received by the co-located antenna pair can be expressed as

$$\mathbf{y(t)} = \begin{bmatrix} y_D(t) \\ y_L(t) \end{bmatrix} = \begin{bmatrix} \sqrt{G_{D,\theta}(\theta,\varphi)}\sin\gamma e^{j\eta} \\ \sqrt{G_{L,\varphi}(\theta,\varphi)}\cos\gamma \end{bmatrix} E \cdot S_0(t). \tag{2}$$

In Eq. (2), $y_D(t)$ and $y_L(t)$ are the signals received by the dipole and loop antennas, respectively. $G_{D,\theta}(\theta,\varphi)$ and $G_{L,\varphi}(\theta,\varphi)$ are $\theta$- and $\varphi$-polarized gains of the dipole and loop antennas, which vary with the incident angles $\theta$ and $\varphi$. $S_0(t)$ is a narrowband phase factor, which can be expressed as

$$S_0(t) = e^{j(\omega_0 t + \psi(t))}, \tag{3}$$

where $\omega_0$ and $\psi(t)$ are the carrier frequency and modulating phase, respectively, for a binary phase-shift keyed (BPSK) signal. The variation of the phase factor does not affect the polarization of the incoming wave, as the phase difference between $E_\theta$ and $E_\varphi$ components remains the same. Thus, we disregard the term of $S_0(t)$ in the following derivation and assume that the incoming wave is not changing during the estimation.
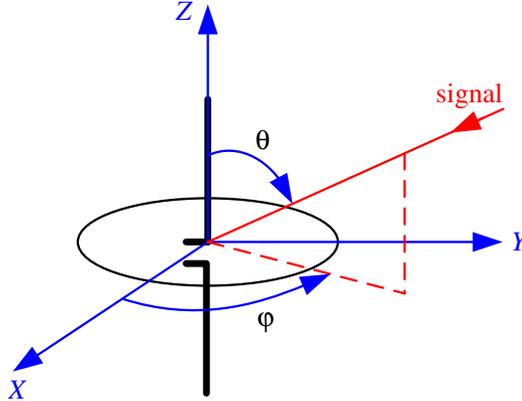


**Figure 1.** A co-located antenna pair with a dipole and a loop antenna.

For practical antennas, due to cross polarization, both the dipole and loop receive $E_\theta$ and $E_\varphi$ components at the same time. Accordingly, without considering the noise, the actual signals received at the dipole and the loop are:

$$\mathbf{y} = \begin{bmatrix} \sqrt{G_{D,\theta}(\theta,\varphi)}\sin\gamma e^{j\eta} + \sqrt{G_{D,\varphi}(\theta,\varphi)}\cos\gamma \\ \sqrt{G_{L,\varphi}(\theta,\varphi)}\cos\gamma + \sqrt{G_{L,\theta}(\theta,\varphi)}\sin\gamma e^{j\eta} \end{bmatrix} E. \tag{4}$$

Thus, to obtain the polarization information without prior information of DOA, the co- and cross-polarized gains for both antennas are required to be angle independent. In view of this, we aim at obtaining omnidirectional patterns for both antennas on the horizontal plane, i.e., the gains are $\varphi$ independent. In this way, the polarization estimation can be carried out on the horizontal plane, with simple calibration performed at only one random angle. Though perfect omnidirectional patterns, including the amplitude and the phase, are not realistic for practical antennas, variations can be reduced so that the estimation accuracy is ensured.

We take an example on the $\theta = 90°$ plane. The calibration is conducted using two linearly polarized plane waves with $\gamma = 90$, $\eta = 0$, and $\gamma = 0$, respectively. The calibrated signals are:

$$
\begin{aligned}
y_{D,\gamma=90} &= \sqrt{G_{D,\theta}(90°,\varphi)}E; \quad y_{L,\gamma=90} = \sqrt{G_{L,\theta}(90°,\varphi)}E; \\
y_{D,\gamma=0} &= \sqrt{G_{D,\varphi}(90°,\varphi)}E; \quad y_{L,\gamma=0} = \sqrt{G_{L,\varphi}(90°,\varphi)}E;
\end{aligned}
\tag{5}
$$

The calibration above takes into account the cross polarization and meanwhile expels the gain imbalance between the dipole and loop, since the absolute gains of the dipole and loop could be different. As the gains are $\varphi$ independent, after the calibration, the signals received by the dipole and loop antennas are represented as:

$$
\mathbf{y(t)} = \begin{bmatrix} y_D \\ y_L \end{bmatrix} = \begin{bmatrix} y_{D,\gamma=90}\sin\gamma e^{j\eta} + y_{D,\gamma=0}\cos\gamma \\ y_{L,\gamma=0}\cos\gamma + y_{L,\gamma=90}\sin\gamma e^{j\eta} \end{bmatrix}.
\tag{6}
$$

It is derived from Eq. (6) that

$$
\tan\gamma e^{j\eta} = \frac{y_{D,\gamma=0}y_L - y_{L,\gamma=0}y_D}{y_{L,\gamma=90}y_D - y_{D,\gamma=90}y_L}.
\tag{7}
$$

As all the received signals are complex, the polarization constants $\gamma$ and $\eta$ can be retrieved from the amplitude and phase information. Other than the plane of $\theta = 90°$, the method can also be utilized when the incident signal is from other horizontal planes, as long as the complex gain ratio between the dipole and loop does not vary with $\theta$.

Assuming that a noise vector, which follows zero-mean circularly-symmetric complex Gaussian distribution and has a covariance matrix of $\sigma^2\mathbf{I}$, is present at each antenna, the output vector of the co-located pair is then given by:

$$
\mathbf{y} = \begin{bmatrix} y_D \\ y_L \end{bmatrix} = \begin{bmatrix} y_{D,\gamma=90}\sin\gamma e^{j\eta} + y_{D,\gamma=0}\cos\gamma \\ y_{L,\gamma=0}\cos\gamma + y_{L,\gamma=90}\sin\gamma e^{j\eta} \end{bmatrix} + \begin{bmatrix} n_D \\ n_L \end{bmatrix}.
\tag{8}
$$

Here the estimation error induced by the noise can be reduced by averaging the received signals. From antenna design perspective, the main challenge is to maintain the omnidirectional patterns for both the amplitude and the phase when the loop is electrically large, and the two antennas are co-located.

## 3. ANTENNA DESIGN AND SIMULATIONS

### 3.1. Antenna Structures and Simulations

The geometries of the co-located antenna pair are presented in Fig. 2. The antenna system consists of a sleeve monopole and a windmill-shaped loop. Compared with the loop in [7], which has four layers and is not easy to fabricate, the loop used in this work only has two conducting layers. The loop antenna is printed on a Rogers RO4003C substrate with a permittivity of 3.48 and thickness of 0.764 mm. On each layer, the circular loop is broken into four curved sections, with each section connected with a radial arm, which shares a common point at the center. The turning directions of the curved sections are opposite on the top and bottom layers. In this way, the currents along the radial arms are opposite on the top and bottom layers, contributing little to the radiated far field. On the contrary, the currents along the circumferential direction form a uniform distribution along the loop. The radius of the loop mainly affects its resonant frequency, whereas the overlap area of the radial arms between the top and bottom layers determines the impedance matching and alters the radiation pattern slightly.
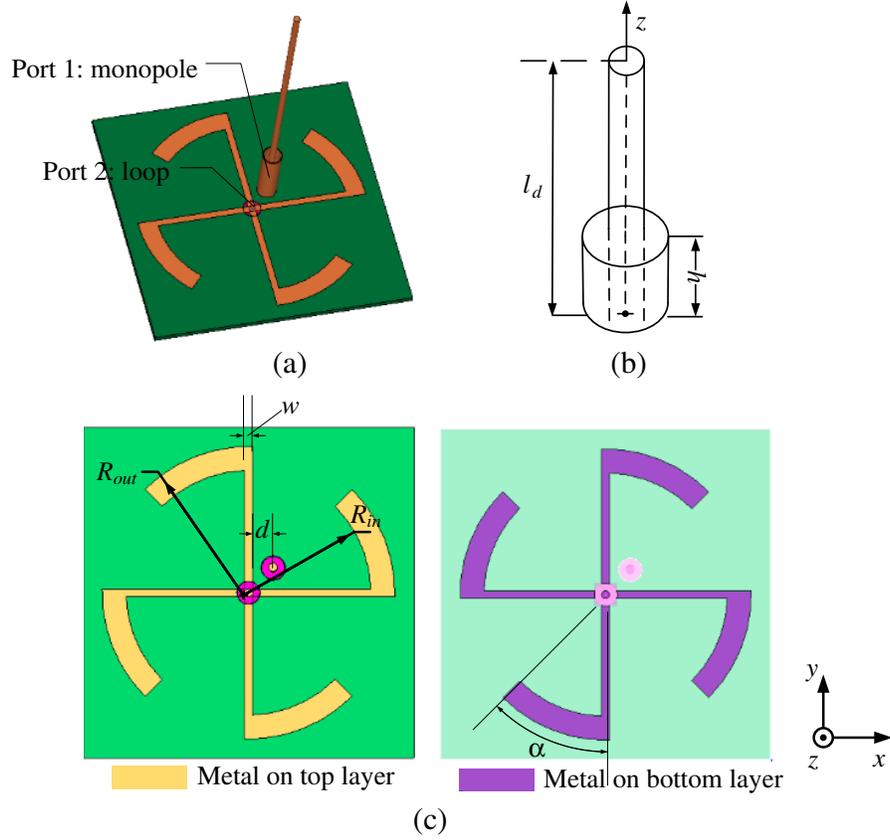
**Figure 2.** (a) 3D view of the proposed antenna system; (b) The configuration of the sleeve monopole; (c) The configuration of the windmill loop. The dimensions are: $L_d = 40$ mm, $h = 9.2$ mm, $R_{out} = 17.7$ mm, $R_{in} = 14.8$ mm, $\alpha = 45°$, $w = 1$ mm, $d = 3$ mm.
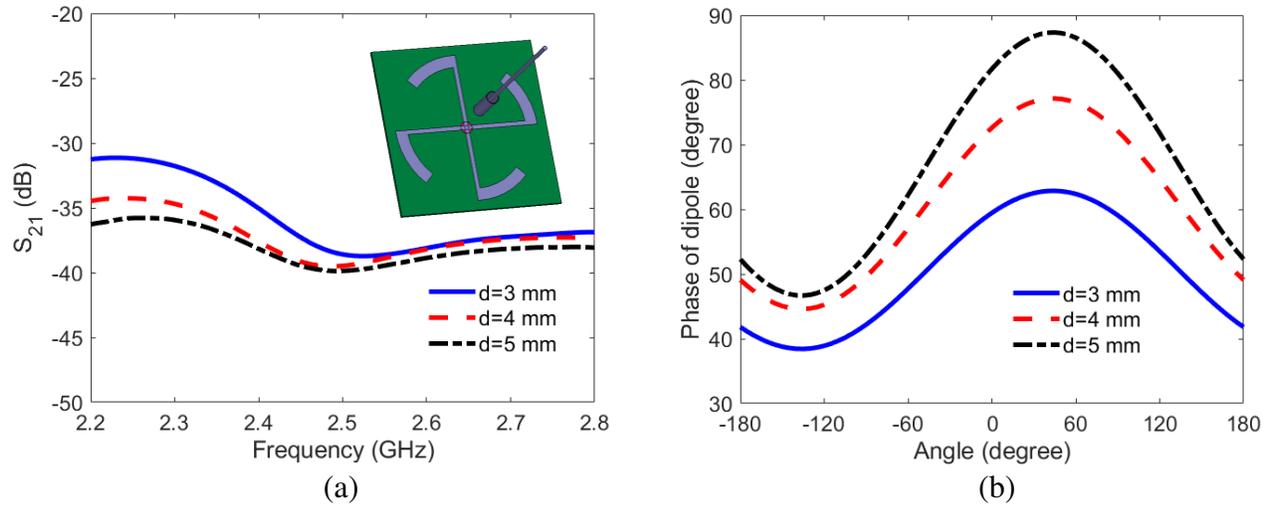


**Figure 3.** The effect of mutual distance on (a) mutual coupling; (b) phase patterns of the sleeve monopole at 2.4 GHz at a distance of 3 m from the antennas.

The distance between the feedings of the loop and the dipole antenna is a key design factor for polarization estimation. Its effect on mutual coupling and pattern deformation is investigated, using the configurations shown in the inset of Fig. 3(a). When the mutual distance becomes large, the mutual

coupling decreases. However, larger mutual distance will deform the phase pattern of the monopole antenna more, as shown in Fig. 3(b), which provides the phase patterns of the sleeve monopole on the $\theta = 90°$ plane, measured at a distance of 3 m from the antennas at 2.4 GHz. The variations of the phases result in inaccuracy during the phase estimation. As the mutual coupling between the antennas is always quite low, smaller mutual distance is preferred for improving the estimation accuracy. In addition, practical factors, such as the accommodation of the SMA connectors, need to be taken into account. As a result, a mutual distance of $d = 3$ mm is determined, which is the smallest possible mutual distance considering physical implementation. It should be noted that the phase pattern of the loop antenna is always very omnidirectional regardless of the variations of the mutual distance.

To reduce the overall dimension and avoid using balun, a sleeve monopole, instead of dipole antenna, along $z$-direction is used to receive $E_\theta$ component. The sleeve with a height of $h$ is added around the monopole and connected to the coat of the coaxial line directly. The small distance between the monopole and the loop can be regarded as being co-located.

Full wave simulations and optimizations were carried out in the time domain using CST Microwave Studio. The $S$-parameters of the loop and sleeve monopole are shown in Fig. 4, which are well matched over the 2.4 GHz band. The port isolation is above 30 dB. As the antennas are of orthogonal polarization, the envelope correlation coefficient (ECC) [19] between the antennas, which is calculated from far field patterns, is around 0.002 at 2.4 GHz. The gain patterns of the monopole and loop antennas on the $xoy$ plane are plotted in Fig. 5. It is observed that the cross polarization level is below $-30$ dB and
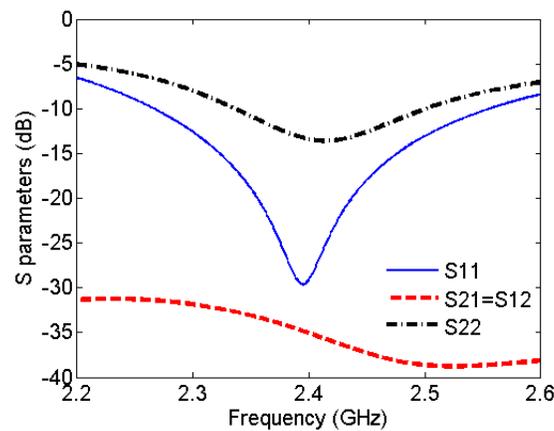


**Figure 4.** The simulated $S$-parameters of the sleeve monopole (port 1) and the windmill loop (port 2).
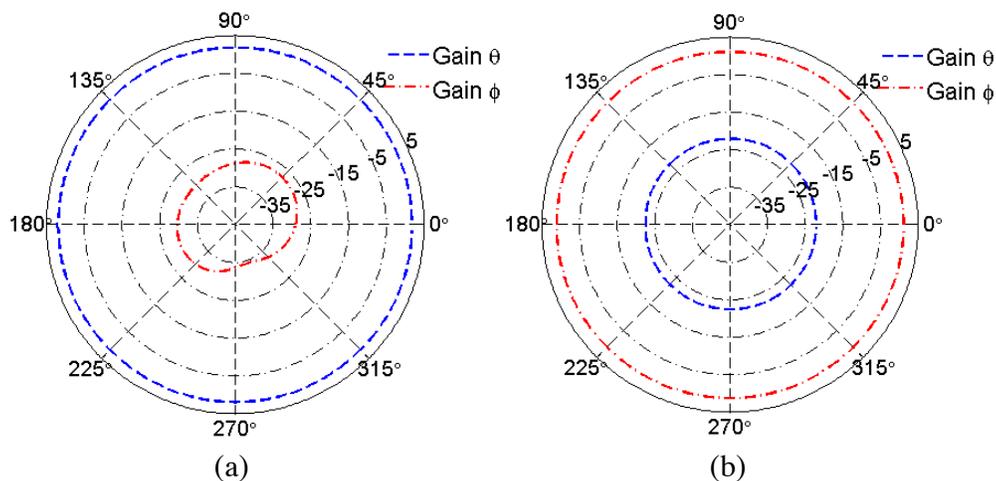


**Figure 5.** The gain patterns of the antennas for (a) the sleeve monopole antenna and (b) the loop antenna.

$-20\,\mathrm{dB}$, respectively, for the monopole and loop antennas. The co-polarized patterns of both antennas and the cross polarized pattern of the loop antenna are omnidirectional. The cross polarized pattern of the monopole antenna is a bit directional, but with very small absolute values.

Due to the low cross polarization, the uniform radiation of the co-polarization is of greater importance. Thus, we show the ratio of the co-polarized $E$-field patterns between the monopole and the loop, i.e., $E_{\theta,\mathrm{dipole}}/E_{\varphi,\mathrm{loop}}$, in Fig. 6(a). The ratios are depicted for the azimuth planes with different elevation angles $\theta$. It is seen that the ratios are almost uniform at the $\theta = 90^\circ$ plane, that is, the ratio is $\varphi$ independent. As $\theta$ decreases, the ratio pattern is tilted a bit, though the variation is very slight. The relative phases in radians between the sleeve monopole and the windmill loop are given in Fig. 6(b) for different horizontal planes, which exhibit even more stable performance than the ratios. Hence, the estimation could be conducted at different elevation planes, but with the accuracy dropping for smaller $\theta$ due to the variation of the ratios. In this paper, we focus on the estimation on the $\theta = 90^\circ$ plane.
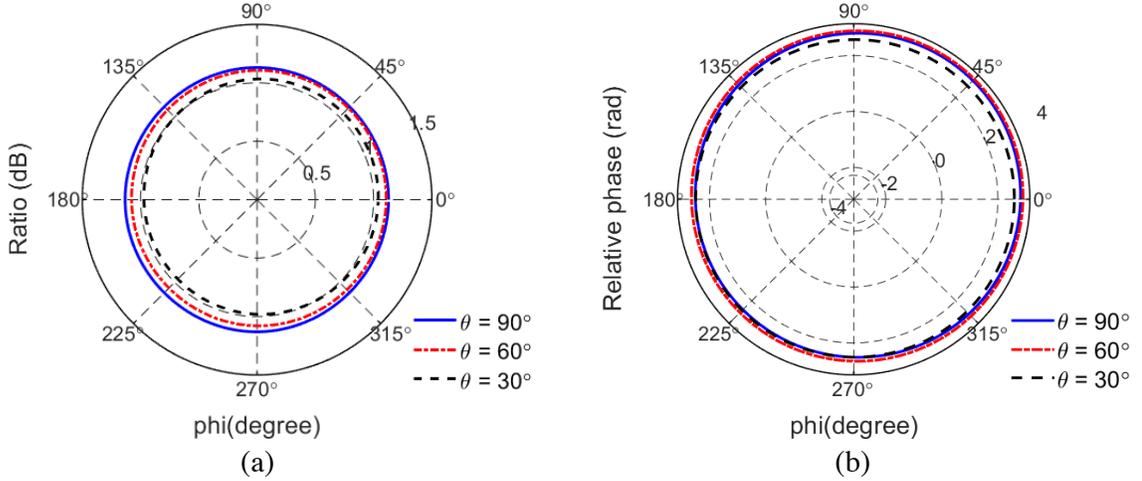


**Figure 6.** (a) The amplitude ratio of the far field patterns between the sleeve monopole and the windmill loop; (b) the relative phase between the sleeve monopole and the windmill loop in radians.

## 3.2. Polarization Estimation

Before the measurement, we verify the polarization estimation in the simulations following the procedure in Section 2. Plane waves of both linear polarization and elliptical polarization are investigated. During the estimation, the plane wave is on the $\theta = 90^\circ$ plane, and the incident angle $\varphi$ is unknown. The signal to noised ratio (SNR) is set to $20\,\mathrm{dB}$. The estimation results of $\tan\gamma$ for the linearly polarized plane waves are shown in Table 1, compared with the corresponding real values. The estimated $\tan\gamma$ is very close to the real values, especially at $\varphi = 90^\circ$ and $\varphi = 180^\circ$ planes. The accuracies at other angles are also high enough for the polarization estimation. The phase difference $\eta$ is either $0^\circ$ or $180^\circ$, which can be well estimated and has not been shown for the concise of the paper.

**Table 1.** Comparison between estimated and real amplitude ratio.

| Real amplitude ratio $\tan\gamma$ | | 0 | 0.56 | 1.732 | Inf. |
|---|---|---|---|---|---|
| Estimated values | $\varphi = 0^\circ$ | 0.07 | 0.50 | 1.69 | 140 |
| | $\varphi = 90^\circ$ | 0.01 | 0.56 | 1.74 | 144 |
| | $\varphi = 180^\circ$ | 0.01 | 0.57 | 1.75 | 160 |
| | $\varphi = 270^\circ$ | 0.07 | 0.52 | 1.69 | 174 |
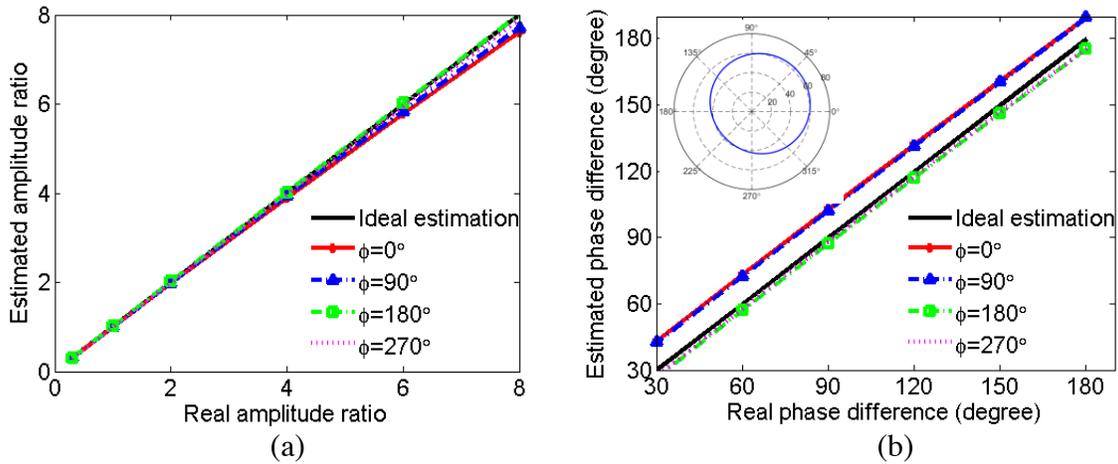
**Figure 7.** Comparison between the estimated and the real polarization information: (a) axial ratio; (b) phase difference. Inset figure: the phase pattern of the sleeve monopole antennas.

The estimation results of the elliptically polarized plane waves, with different axial ratios and phase differences, are presented in Figs. 7(a) and (b), respectively. Axial ratios are estimated with the phase difference being 60°, whereas the phase differences are estimated when the axis ratio is fixed at 4. It is seen that the axial ratios are well estimated at any incident angle, with a bit larger discrepancy when the ratios become higher. The phase shift $\eta$ is accurately estimated for $\varphi = 180°$ and $\varphi = 270°$, whereas a 10° discrepancy appears for $\varphi = 0°$ and $\varphi = 90°$. This can be explained by the phase center shifting of the monopole, as depicted in the inset of Fig. 7(b). In the simulations, the calibration is carried out at the angle of $\varphi = 150°$, as its phase is close to the averaged phase. Since the phases of the monopole at $\varphi = 0°$ and $\varphi = 90°$ deviate from that at $\varphi = 150°$, the accuracy of phase estimation deteriorates at those angles. It is noted from Fig. 7(b) that the phase variation of the sleeve monopole is around 20° in total, and the estimation inaccuracy of the phase is only 10°. This is because the phase of the incident wave does not vary linearly with the phase of the antenna, as given in Eq. (7). The estimation accuracy can be improved when the phase pattern and the direction of arrival are known.

## 4. ANTENNA MEASUREMENT AND RESULTS

A prototype was fabricated (see Fig. 8) and then measured with Agilent N5221A network analyzer. The loop antenna is directly connected with a 50 Ω SMA connector, whose pin and flange are soldered with the top and bottom strip lines, respectively. The lengths of the coaxial cables for the two antennas are kept the same to eliminate the phase shift from the ports. To accommodate the measurement cable, the SMA cable of the loop is bent a bit, which makes its connection to the bottom layer not exactly at the center, resulting in a small deterioration of the cross polarization. The measured $S$-parameters are plotted in Fig. 9. The two antennas maintain good impedance matching at 2.4 GHz, though the resonant frequency of the loop antenna is shifted to higher band by around 100 MHz.

Before the polarization estimation experiment, the axial ratio of a commercially used WLAN antenna, as shown in the inset of Fig. 11, was measured at the horizontal plane using horn antenna HP970 in an anechoic chamber. An axial ratio of 15.6 dB is obtained. The measurement setups are shown in Fig. 10. The distance between the antennas is set to 2 meters. The same horn antenna was then used to calibrate the co-located antenna system at the angle of $\varphi = 150°$, as in the simulation. The complex transmission coefficients between the horn antenna and co-located antennas were measured at 2.4 GHz when the horn antenna was horizontally and vertically placed, respectively. Afterwards, the WLAN antenna was used as the transmitter, and the proposed co-located antenna system was employed as the receiver (see the bottom picture in Fig. 10). The WLAN antenna is moved around the co-located antennas so that different incident angles from 0° to 180° are realized. The obtained complex transmission coefficients, together with the calibrated values, were processed according to Eq. (7) to
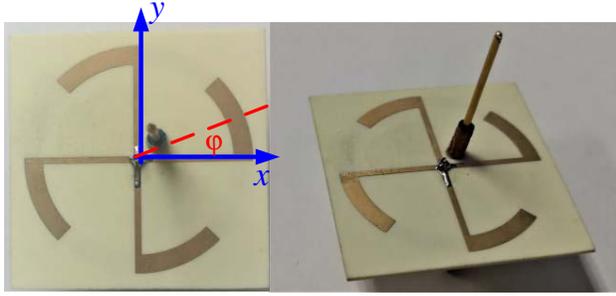
**Figure 8.** Prototype of the co-located antenna system for polarization estimation.
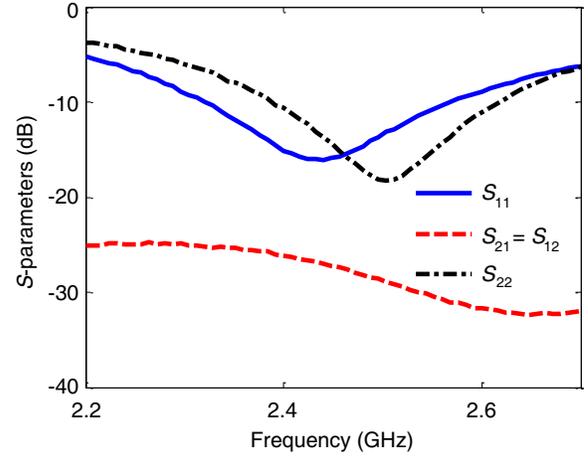


**Figure 9.** Measured $S$-parameters of the co-located antenna system. (Port 1: the sleeve monopole; port 2: the windmill loop).
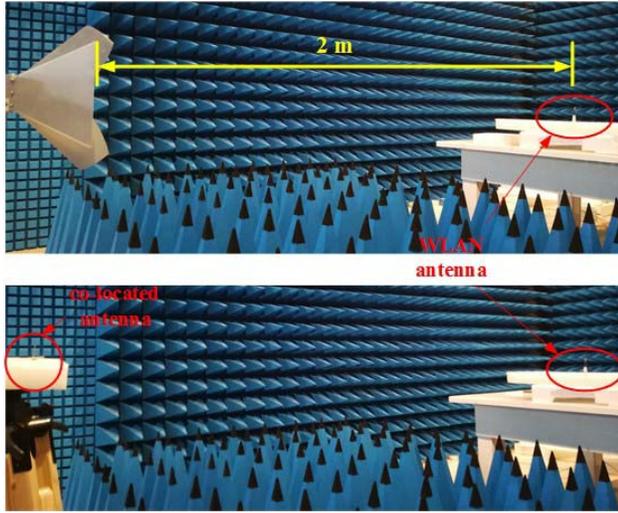


**Figure 10.** The antenna setup for measuring the polarization information of the WLAN antenna.
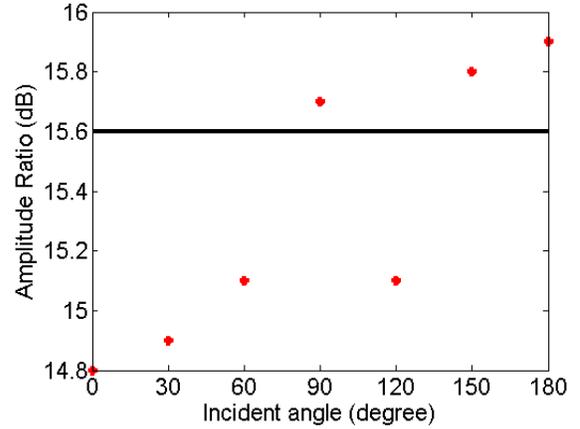


**Figure 11.** Estimated axis ratios of the WLAN antenna using the co-located antennas.

estimate the axial ratio. The estimated axial ratio in dB scale is presented in Fig. 11 for different incident angles. In general, the axial ratios were reasonably estimated. The variations are mainly due to the asymmetrical structure of the co-located antennas and the existence of the cables. Besides, the WLAN antenna might not be ideally omnidirectional, and the angle of the WLAN antenna facing the co-located antennas is not always the same when its relative angle to the co-located antennas is changed. This leads to axial ratio variations of the incident waves.

## 5. CONCLUSIONS

This work proposes a co-located antenna pair consisting of a windmill loop and a sleeve monopole antenna. The antennas can be used for polarization estimation without pattern calibration, as they share the same radiation pattern but orthogonal polarizations. The procedures of polarization estimation have been described in the paper, taking into account the cross polarization of practical antennas. The method has been validated using incident waves with linear and elliptical polarizations. The prototype

of the co-located antenna pair was fabricated and used to estimate the polarization information of a commercial WLAN antenna in an anechoic chamber. Good estimation accuracy has been achieved when signals are from different directions.

## ACKNOWLEDGMENT

## REFERENCES

1. Tian, Y., B. Wen, J. Tan, and Z. Li, "Study on pattern distortion and DOA estimation performance of crossed-loop/monopole antenna in HF radar," *IEEE Trans. Antennas Propag.*, Vol. 64, No. 11, 6095–6106, Nov. 2017.

2. Slater, M. J., C. D. Schmitz, M. D. Anderson, D. L. Jones, and J. T. Bernhard, "Demonstration of an electrically small antenna array for UHF direction-of-arrival estimation," *IEEE Trans. Antennas Propag.*, Vol. 61, No. 3, 1371–1377, Mar. 2013.

3. Pralon, M. G., G. D. Daldo, M. Landmann, M. A. Hein, and R. S. Thoma, "Suitability of compact antenna arrays for direction of arrival estimation," *IEEE Trans. Antennas Propag.*, Vol. 65, No. 12, 7244–7256, Dec. 2017.

4. Li, H., S. Sun, and J. Wang, "Direction of arrival estimation using amplitude and phase information in low-profile MIMO arrays," *IEEE Trans. Antennas Propag.*, Vol. 66, No. 11, 6457–6462, Aug. 2018.

5. Liu, Y. and L. Huang, "Pattern compensation for DOA estimation by electromagnetic vector sensors," *Proc. International Conf. Microwaves, Radar and Wireless Communications (MIKON)*, Gdansk, Poland, 2014.

6. Balanis, C. A., *Antenna Theory — Analysis and Design,* 3rd Edition, John Wiley & Sons, 2005.

7. Kim, D. S., C. H. Ahn, Y. T. Im, S. J. Lee, K. C. Lee, and W. S. Park, "A Windmill-shaped loop antenna for polarization diversity," *Proc. IEEE Antennas Propag. Soc. Int. Symp.*, 361–364, Honolulu, Jun. 2007.

8. Wong, K. T., L. Li, and M. D. Zoltowski, "Root-MUSIC-based direction-finding and polarization estimation using diversely polarized possibly collocated antennas," *IEEE Antennas Wireless Propag. Lett.,* Vol. 3, 129–132, 2004.

9. Yuan, X., K. T. Wong, and K. Agrawal, "Polarization estimation with a dipole-dipole, a dipole-loop, or a loop-loop pair of various orientations," *IEEE Trans. Antennas Propag.*, Vol. 60, No. 5, 2442–2452, May 2012.

10. Xuan, X., "Spatially spread dipole/loop quads/quints: For direction finding and polarization estimation," *IEEE Antennas Wireless Propag. Lett.,* Vol. 12, 1081–1084, 2013.

11. Shen, L., Z. Liu, and Y. Xu, "Parameter estimation using partly calibrated vector antennas," *IEEE Antennas Wireless Propag. Lett.,* Vol. 16, 860–863, 2017.

12. Best, S. R., "The electrically small dipole-loop pair revisited," *Proc. IEEE Antennas Propag. Society Int. Symp.*, 2265–2268, 2007.

13. Kim, J. and Y. Rahmat-Samii, "Integrated low-profile dual loop-dipole antennas using an embedded electromagnetic bandgap structure," *Microw. Opt. Technol. Lett.,* Vol. 49, No. 5, 1085–1089, May 2007.

14. Wong, K. T., Y. Song, C. J. Fulton, S. Khan, and W. Y. Yam, "Electrically 'long' dipoles in a collocated orthogonal triad — For direction finding and polarization estimation," *IEEE Trans. Antennas Propag.*, Vol. 65, No. 11, 6057–6067, Nov. 2017.

15. Khan, S., K. T. Wong, Y. Song, and W. Y. Tam, "Electrically large cirlular loops in the estimation of an incident Emitter's direction of arrival or polarization," *IEEE Trans. Antennas Propag.*, Vol. 66, No. 6, 3046–3055, Jun. 2018.

16. Ebihara, S., A. Uemura, T. Kuroda, and H. Soda, "Dipole array antenna and loop antenna for estimation of direction and polarization in borehole radar," *Proc. 15th International Conference on Ground Penetrating Radar*, 780–784, Brussels, Belgium, Jun. 2014.

17. Duplouy, J., C. Morlaas, H. Aubert, P. Potier, P. Pouliguen, and C. Djoma, "Reconfigurable grounded vector antenna for 3D electromagnetic direction finding applications," *IEEE Antennas Wireless Propag. Lett.,* Vol. 17, No. 2, 197–200, 2018.

18. Xiong, J., M. Zhao, H. Li, Z. Ying, and B. Wang, "Collocated electric and magnetic dipoles with extremely low correlation as reference antenna for polarization diversity MIMO applications," *IEEE Antennas Wireless Propag. Lett.,* Vol. 11, 423–426, 2012.

19. Blanch, S., J. Romeu, and I. Corbella, "Exact representation of antenna system diversity performance from input parameter description," *Electron. Lett.,* Vol. 39, No. 9, 705–707, May 2003.